Journal of Magnetic Resonance 198 (2009) 197–203

Contents lists available at ScienceDirect

Journal of Magnetic Resonance

journal homepage: www.elsevier.com/locate/jmr

Double quantum transition as the origin of the central dip in the *z*-spectrum of HDO in variably stretched gel

Uzi Eliav [a], Christoph Naumann [b], Gil Navon [a], Philip W. Kuchel [b,*]

[a] School of Chemistry, Tel-Aviv University, Ramat Aviv 69987, Israel
[b] School of Molecular and Microbial Biosciences, University of Sydney, Building G08, NSW 2006, Australia

ARTICLE INFO

Article history:
Received 19 December 2008
Revised 13 February 2009
Available online 21 February 2009

Keywords:
Anisotropy
Density matrix
Double quantum transition
High-rank tensor relaxation
^{2}H NMR
D_2O
Liouville–von-Neumann equation
Residual quadrupolar coupling
Stretched gelatin

ABSTRACT

The ^{2}H NMR spectrum of HDO in gelatin gel, that is stretched inside silicone rubber tubing, displays a well resolved doublet. Spectra were obtained with a range of offset frequencies of partially saturating radio-frequency (RF) radiation. The resulting steady-state irradiation envelope (also referred to as a '*z*-spectrum') has the peculiar feature that maximal suppression of the doublet occurs when the irradiation is applied exactly at the centre frequency, between the two HDO peaks. We present a quantum mechanical explanation for this phenomenon. It is shown that the phenomenon is the result of double quantum transitions. The analysis is extendable to more complex quadrupolar and dipolar-coupled systems of other nuclides. It has implications for enhancement of contrast in magnetic resonance imaging of heterogeneous systems using dipolar and quadrupolar interactions.

1. Introduction

Magnetization transfer is the basis of several contrast-enhancement methods used in magnetic resonance imaging (notably CEST [1]; and PARACEST [2]). It relies on the saturation of the magnetization of one spin population and monitoring the effect on another. In a variant of these types of experiments, but now involving a quadrupolar nucleus, radio-frequency (RF) radiation, is applied at offsets across the whole ^{2}H NMR spectrum of HDO in a stretched gel. This invokes the most marked suppression, not when applied to one or other of the two obvious peaks, but when applied exactly in the centre between them [3]. In this paper, we provide a quantum mechanical explanation for this phenomenon.

The ^{2}H NMR peak splitting is attributed to the interaction of the electric quadrupole of the spin-1 ^{2}H nucleus with the average electric field gradient tensor of the partially aligned polymers (gelatin) in the stretched gel [4]. The magnitude of this residual quadrupolar coupling is, to a very good approximation, linear with the extent of stretching [4]; this behaviour has proved useful in applying the aligned, chiral system to resolving spectra of mixtures of optical isomers [5,6]. The gel also forms the basis of a new means of measuring the rate of exchange of water between the inside and outside of erythrocytes (red blood cells; RBCs) [3]. In the experiment, the intracellular HDO has no apparent splitting, while the HDO outside does. However, during the development of this new approach we observed the phenomenon noted above; and as a consequence we needed to modify the conventional saturation-transfer experiment that is often applied in situations where there are separate resonances from two exchanging populations of spins [3].

Residual dipolar and quadrupolar interactions in spin systems lead to the formation of high-rank tensors ($T_{l,\pm1}$, $l = 2,\ldots,2I$; where I is the spin-quantum number of the nucleus) [7–11]; and these interactions are of interest in characterising ordered biological tissues such as cartilage and tendons, and can be detected in NMR spectra by multiple-quantum filtering [12–18].

Our interpretation of the steady-state irradiation envelope stems from the formation of high-rank tensors under such irradiation conditions and it is closely related to approaches presented by Hatanaka et al. [19,20], Vega and Pines et al. [7–9,21,22], and Bain et al. [23–25] where such tensors were formed by selective pulses. The average Liouvillian theory that we used in the current work has recently been reviewed by Ghose [26]. The use of the spherical tensor operator basis of Hilbert space of quadrupolar spins relies on the foundational work of Müller et al. [27], and Chung and Wimperis [28].

* Corresponding author. Fax: +61 2 9351 4726.
E-mail address: p.kuchel@mmb.usyd.edu.au (P.W. Kuchel).

1090-7807/$ - see front matter © 2009 Elsevier Inc. All rights reserved.
doi:10.1016/j.jmr.2009.02.006

2. Methods

2.1. Theory

2.1.1. Density matrix

In spin space (Hilbert space) the density operator contains all the information about the spin system (e.g., [23–26]). The equations of motion of the density operator (the caret denotes an operator) is given by the Liouville–von-Neumann equation [29]:

$$\frac{d\hat{\rho}}{dt} = -i[\hat{H}, \hat{\rho}] \tag{1}$$

where $\hat{\rho}$ is the density operator, and $\hat{H}$ is the Hamiltonian operator. If relaxation is included in the system, Eq. (1) becomes:

$$\frac{d\hat{\rho}}{dt} = -i[\hat{H}, \hat{\rho}] - \hat{\hat{R}}\ (\hat{\rho} - \hat{\rho}_{eq}) \tag{2}$$

where, $\hat{\hat{R}}$ is the Redfield relaxation operator that operates on $\hat{\rho}$; i.e., it is a super-operator, hence the use of double carets.

In the present system the expression for $\hat{H}$ is:

$$\hat{H} = \omega_1 \hat{I}_x + (1/3)\ \omega_Q\ (3\hat{I}_z^2 - I^2) + \delta\omega \hat{I}_z \tag{3}$$

where, ω_1 is the magnitude in frequency units of the B_1 radio-frequency (RF) magnetic field; $\hat{I}_x$ is the x-axis spin operator; ω_Q is the residual quadrupolar coupling constant (note that in this work it is half the frequency difference between the two components of the doublet); $\hat{I}_z$ is the z-axis spin operator; I is the spin-quantum number of the nucleus; and $\delta\omega$ is the offset frequency of the B_1 RF field.

The commutator in Eq. (2) can be represented as a super-operator that operates on $\hat{\rho}$, and is called the Liouvillian:

$$\hat{\hat{L}} = [\hat{H}, \_] \tag{4}$$

Hence, Eq. (2) takes the form:

$$\frac{d\hat{\rho}}{dt} = -i\ \hat{\hat{L}}\ \hat{\rho} - \hat{\hat{R}}\ (\hat{\rho} - \hat{\rho}_{eq}) \tag{5}$$

If the RF field is applied continuously for sufficiently long before acquisition of a free-induction decay (FID), the energy of the system reaches a steady state, which is a balance between energy input from the RF field and loss to the lattice via relaxation. Thus, the derivative on the left hand side of Eq. (5) becomes 0. By rearranging this equation, we obtain the expression for the steady-state density matrix, $\hat{\rho}_{ss}$:

$$\hat{\rho}_{ss} = -(i\hat{\hat{L}} + \hat{\hat{R}})^{-1}\hat{\hat{R}}\ \hat{\rho}_{eq} \tag{6}$$

where $\hat{\rho}_{eq}$ is the density matrix at magnetization equilibrium.

The matrix representation of the Liouvillian (commutator of the Hamiltonian in operator or Liouville space) is obtained from the expression:

$$\hat{\hat{L}}\ \hat{O}_i = -i[\hat{H}, \hat{O}_i] = \sum_j^N H_{ij}\ \hat{O}_i \tag{7}$$

where the $\hat{O}_i$ are basis operators. In the present system, where any value for the ratio ω_1/ω_Q is possible, and thus the dimension of our tensors space is 8×8, we have chosen the irreducible spherical tensors as a basis, $T_{l,p}$ (e.g., [30–32]) and the $H_{i,j}$ are elements of the matrix of the Liouvillian and are formally given by:

$$\langle \hat{O}_i \mid \hat{\hat{L}} \mid \hat{O}_j \rangle = tr\left(\hat{O}_i \cdot \hat{\hat{L}} \cdot \hat{O}_j\right) \tag{8}$$

However, $H_{i,j}$ can be calculated directly from evaluating the commutator $[\hat{H}, \hat{O}_i]$ while noting that the result is a superposition of the basis operators. Specifically, the RF part of the Hamiltonian is written as

$$\hat{H}_{RF} = \omega_1\ (\hat{I}_+ + \hat{I}_-)/2 \tag{9}$$

and the commutator is:

$$[\hat{H}_{RF}, \hat{I}_z] = \omega_1\ (T_{1,1} + T_{1,-1})/\sqrt{2} \tag{10}$$

Hence the matrix element that connects $\hat{I}_z$ and $T_{1,1}$ and $T_{1,-1}$ is $-i\omega_1/\sqrt{2}$. The other parts of the Hamiltonian in Eq. (3) are related to the basis operators in a similar way.

Any operator can be represented as a column vector; e.g., $\hat{I}_z$={0,1,0,0,0,0,0,0}. Thus the Liouvillian can be represented in matrix form, where the term in round brackets is the matrix of column vectors that correspond to the irreducible spherical tensors, where the relaxation-rate-constant matrix is:

$$\begin{array}{c} \\ T_{1,-1} \\ T_{1,0} \\ T_{1,1} \\ T_{2,-2} \\ T_{2,-1} \\ T_{2,0} \\ T_{2,1} \\ T_{2,2} \end{array} \begin{array}{c} \begin{array}{cccccccc} T_{1,-1} & T_{1,0} & T_{1,1} & T_{2,-2} & T_{2,-1} & T_{2,0} & T_{2,1} & T_{2,2} \end{array} \\ \begin{pmatrix} -R_2 & & & & & & & \\ & -R_1 & & & & & 0 & \\ & & -R_2 & & & & & \\ & & & -R_{DQ} & & & & \\ & & & & -R_3 & & & \\ & & & & & -R_{ZQ} & & \\ & 0 & & & & & -R_3 & \\ & & & & & & & -R_{DQ} \end{pmatrix} \end{array} \tag{11}$$

and $i\hat{\hat{L}} + \hat{\hat{R}}$ in Eq. (6) has the following form:

$$\begin{array}{c} \\ T_{1,-1} \\ T_{1,0} \\ T_{1,1} \\ T_{2,-2} \\ T_{2,-1} \\ T_{2,0} \\ T_{2,1} \\ T_{2,2} \end{array} \begin{array}{c} \begin{array}{cccccccc} T_{1,-1} & T_{1,0} & T_{1,1} & T_{2,-2} & T_{2,-1} & T_{2,0} & T_{2,1} & T_{2,2} \end{array} \\ \begin{pmatrix} -R_2 + i\delta\omega & -\sqrt{2}i\omega_1/2 & 0 & 0 & -i\omega_Q & 0 & 0 & 0 \\ -\sqrt{2}i\omega_1/2 & R_1 & -\sqrt{2}i\omega_1/2 & 0 & 0 & 0 & 0 & 0 \\ 0 & -\sqrt{2}i\omega_1/2 & -R_2 - i\delta\omega & 0 & 0 & 0 & i\omega_Q & 0 \\ 0 & 0 & 0 & -R_{DQ} + i\delta\omega & -i\omega_1 & 0 & 0 & 0 \\ -i\omega_Q & 0 & 0 & -i\omega_1 & -R_3 + i\delta\omega & -\sqrt{3/2}i\omega_1 & 0 & 0 \\ 0 & 0 & 0 & 0 & -\sqrt{3/2}i\omega_1 & -R_{ZQ} & -\sqrt{3/2}i\omega_1 & 0 \\ 0 & 0 & i\omega_Q & 0 & 0 & -\sqrt{3/2}i\omega_1 & -R_3 - i\delta\omega & -i\omega_1 \\ 0 & 0 & 0 & 0 & 0 & 0 & -i\omega_1 & -R_{DQ} - i2\delta\omega \end{pmatrix} \end{array} \tag{12}$$

The expectation value of $\langle T_{1,0}\rangle = \langle \hat{I}_z\rangle$ (z-magnetization) is given by the scalar product of the transpose of the vector representation of $\hat{I}_z$ (shown above) and the result of multiplying the inverse of the matrix in Eq. (12), and $\mathbf{I}_z$ (where the bold symbol represents a matrix or a vector according to the context). The matrix was programmed in *Mathematica* [33] and it was inverted and multiplied by the column $\{0,-R_1,0,0,0,0,0,0\}$, all executions being symbolic. Thus

$$\langle \hat{I}_z\rangle = \mathbf{I}_z^{\text{transpose}} \cdot \boldsymbol{\rho}_{ss} = A/(A+B)$$

where the expressions for A and B, derived in *Mathematica* [33] are:

$$\begin{aligned}A = R_1\Big\{ & R_{DQ}^2 R_{ZQ}\delta\omega^4 + 4R_{ZQ}\delta\omega^6 + R_3^2 R_{ZQ}\delta\omega^2(R_{DQ}^2+4\delta\omega^2)\\ & -4R_{ZQ}\delta\omega^4\omega_1^2 + R_3\delta\omega^2\left(3R_{DQ}^2+2R_{DQ}R_{ZQ}+12\delta\omega^2\right)\omega_1^2\\ & +3R_{DQ}\delta\omega^2\omega_1^4 + R_{ZQ}\delta\omega^2\omega_1^4 + R_2^2\Big[R_{DQ}^2R_{ZQ}\delta\omega^2 + R_3^2R_{ZQ}\left(R_{DQ}^2+4\delta\omega^2\right)\\ & +R_3\left(3R_{DQ}^2+2R_{DQ}R_{ZQ}+12\delta\omega^2\right)\omega_1^2 + 3R_{DQ}\omega_1^4 + R_{ZQ}\left(-2\delta\omega^2+\omega_1^2\right)^2\Big]\\ & -2R_{DQ}^2R_{ZQ}\delta\omega^2\omega_Q^2 - 8R_{ZQ}\delta\omega^4\omega_Q^2 + 4R_{ZQ}\delta\omega^2\omega_1^2\omega_Q^2\\ & +R_2\Big[2R_3R_{ZQ}\left(R_{DQ}^2+4\delta\omega^2\right)+\left(3R_{DQ}^2+2R_{DQ}R_{ZQ}+12\delta\omega^2\right)\omega_1^2\Big]\omega_Q^2\\ & +R_{DQ}^2R_{ZQ}\omega_Q^4 + 4R_{ZQ}\delta\omega^2\omega_Q^4\Big\}\end{aligned}$$

and

$$\begin{aligned}B = \omega_1^2\Big\{ & R_2\Big[R_{DQ}^2R_{ZQ}\delta\omega^2 + R_3^2R_{ZQ}\left(R_{DQ}^2+4\delta\omega^2\right)\\ & +R_3\left(3R_{DQ}^2+2R_{DQ}R_{ZQ}+12\delta\omega^2\right)\omega_1^2 + 3R_{DQ}\omega_1^4\\ & +R_{ZQ}\left(-2\delta\omega^2+\omega_1^2\right)^2\Big] + R_{ZQ}\Big[R_3\left(R_{DQ}^2+4\delta\omega^2\right)+R_{DQ}\omega_1^2\Big]\omega_Q^2\Big\}\end{aligned} \tag{13}$$

In subsequent evaluations, we made the substitutions of radial frequencies to those in Hz, namely $\nu_1 = \omega_1/2\pi$, $\delta\nu = \delta\omega/2\pi$, and $\nu_Q = \omega_Q/2\pi$.

2.1.2. Mathematica programming

Eq. (13) was derived analytically, and evaluated numerically, on the 'few-second' time scale, in *Mathematica* [33] (installed on a Macintosh MacBook Pro with 2 GB of memory, running at 2.16 GHz) for a set of input parameter values as indicated below and in the relevant figure captions.

2.2. Gels

In its liquid state (usually at 40–80 °C) gelatin (Gelita, Brisbane, Qld, grade 20N) solution (30–50% w/v in 100% D_2O) was drawn into a silicone rubber tube (for 5-mm NMR tubes Silastic® laboratory tubing by Dow Corning Corporation; Cat. No. 508-009, 1.98 mm i.d., 3.18 mm o.d.) that was sealed with a plug at one end, as previously described [6]. This tube was then inserted into a glass tube (5 mm o.d.) so that when the gel formed (at less than ~30 °C) it could be stretched inside the silicone tube, and held extended by a thumbscrew that was positioned at the upper end of the outer glass tube.

2.3. NMR

2.3.1. Spectrometer and data processing

^{2}H NMR spectra were recorded at 61.42 MHz on a Bruker DRX 400 spectrometer (Bruker, Karlsruhe, Germany) with an Oxford Instruments (Oxford, UK) 9.4 T, vertical, wide-bore magnet, and at 76.77 MHz on a Bruker DRX 500 spectrometer 11.7 T, vertical, narrow-bore magnet.

Gaussian–Lorentzian deconvolution (Bruker, TopSpin 2.0, release March 21, 2007) or manual integration were used, as relevant, to extract the relative areas of resonances in one-dimensional spectra.

2.3.2. Pulse sequences

For the saturation envelopes (z-spectra) the pulse sequence entailed a period of low power, variable offset irradiation, followed by a phase cycled $\pi/2$ pulse, then acquisition of the free-induction decay. Selective irradiation was achieved with a pulse of 0.5–1.0 s duration using a power-attenuation of ~50–60 dB from a standard Bruker 300 W decoupling amplifier. The value of the attenuation factor was initially adjusted empirically to achieve full signal suppression of the HDO signal in the unstretched state of the sample. In other experiments the attenuation was set so that incomplete saturation was achieved. We varied the irradiation frequencies in small steps throughout the whole spectrum to one for which there was no longer any peak suppression. After standard 1D processing, all spectra were integrated. Each integral was plotted in Fig. 1 as a percentage of that of the corresponding nonsaturated spectrum.

The longitudinal relaxation time T_1 of the tensor $T_{1,0}$ ($\hat{I}_z$), and longitudinal relaxation time T_{ZQ} of the tensor $T_{2,0}$, were measured from spectra acquired with the following pulse sequence: $d1$ (low power RF with variable offset from resonance)—$t_1 - \beta(\varphi_1)$ – acquire (t_2), with a coherent-magnetization-dispersing field gradient pulse ('crusher pulse') applied at the beginning of t_1. The saturation pulse was applied to the satellite peaks with a power less than 100 Hz so that the steady-state values of the tensors $T_{1,0}$ and $T_{2,0}$ (denoted by $\rho_{T_{1,0}}$ and $\rho_{T_{2,0}}$, respectively) were not negligible. After t_1, and applying the hard pulse of flip angle β the FID was acquired. It followed the expression (assuming that all single quantum tensors relax with the same rate constant, and M_{eq} denotes equilibrium magnetization.):

$$\begin{aligned}\text{FID}(t_2) = {} & d^1_{-1,0}(\beta)[(\rho_{T_{1,0}} - M_{eq})e^{-t_1/T_1} + M_{eq}]e^{-t_2/T_2}\cos(\omega_Q t_2)\\ & + d^2_{-1,0}(\beta)\rho_{T_{2,0}}e^{-t_1/T_{ZQ}}e^{-t_2/T_2}\sin(\omega_Q t_2)\end{aligned} \tag{14}$$

where $d^1_{-1,0}(\beta)$ and $d^2_{-1,0}(\beta)$ are the Wigner 'small d' matrices that describe the transfer of the tensors $T_{1,0}$ and $T_{2,0}$ into $T_{1,-1}$ and $T_{2,-1}$ by the hard pulse of angle β. The Fourier transform of the expression in Eq. (14) is a superposition of a symmetric (in-phase) part, the first term on the right hand side, and an anti-symmetric (anti-phase) part, yielding an overall asymmetric spectrum. The dependence of the symmetric part on t_1 yields T_1, while the asymmetric part gives T_{ZQ}. The symmetric and anti-symmetric parts are separated by running the above pulse sequence twice, once with $\beta = \pi/4$ and then with $\beta = 3\pi/4$, and adding and subtracting the results; the in-phase spectrum was obtained by addition since $d^1_{-1,0}(\pi/4) = d^1_{-1,0}(3\pi/4)$ while the anti-phase spectrum was the result of subtraction because $d^2_{-1,0}(\pi/4) = -d^2_{-1,0}(3\pi/4)$.

The measurement of the double-quantum transverse relaxation time T_{DQ} of the tensor $T_{2,2}$ was made using the pulse sequence: $\pi/2(\varphi_1) - \tau/2 - \pi/2(\varphi_2) - t_{DQ} - \pi/2(\varphi_3) - \tau/2 - \pi/2(\varphi_4) - t_{LM} - \pi/2(\varphi_5)$ – acquire($t_2, \varphi_{\text{receiver}}$), where the phases ($\varphi$) of the RF pulses were chosen to select the magnetization-coherence pathway that led to $T_{2,2}$ and $T_{2,-2}$ in the time interval t_{DQ}; and t_{LM} is a delay, for which the subscript LM denotes longitudinal magnetization. The dependence of the signal intensity on t_{DQ} was analysed with a single exponential fit to give the estimate of T_{DQ}.

The transverse relaxation time for the tensors, $T_{1,1}$, and $T_{2,1}$, was measured using the pulse sequence: $\pi/2(\varphi_1) - \tau/2 - \pi/2(\varphi_2) - \tau/2$ – acquire($t_2, \varphi_{\text{receiver}}$), measuring the signal intensity for 10 different values of τ. The two corresponding transverse relaxation-rate constants used in Eq. (13), R_2 and R_3, were assumed in the first instance to have a similar value hence the measurement of a single (combined) relaxation time T_2; however, this is not a general result (see Section 4.1).

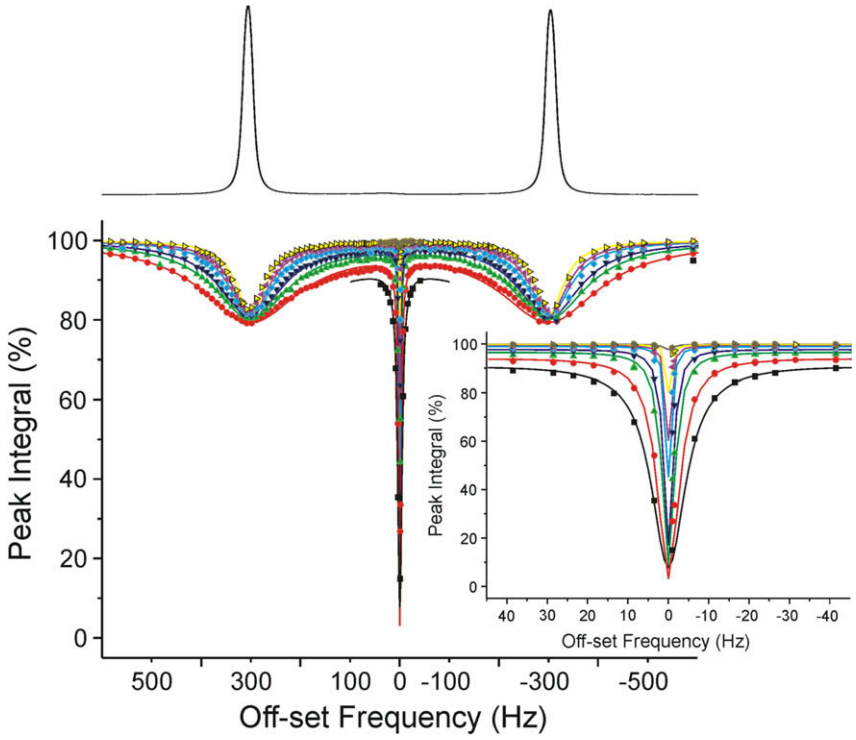

Fig. 1. ^{2}H NMR (61.422 MHz) steady-state irradiation envelopes (*z*-spectra; % integral of control spectrum) of HDO in stretched gelatin gel, and the effect of applying selective RF irradiation with a range of magnitudes to the ^{2}H spins. The envelopes were derived from changing the offset frequency of the applied RF radiation on the total ^{2}H NMR signal intensity (integral) while the corresponding starting spectra were obtained without any selective irradiation. The sample of gelatin was prepared from 50% (w/v) bovine gelatin with 100% (w/v) pure D_2O. The value of ν_Q was found to be 300 Hz (half the splitting between the two peaks) with the particular extent of stretching used (0.7), and the values fitted (solid lines) to the relaxation parameters using Eq. (13) were set to be the same for all *z*-spectra in the series after iterative processing that focussed on the spectrum with ν_1 = 38 Hz: T_1 = 100.1 ms; T_2 = 40.7 ms; $(1/R_3) = T_3$ = 40.7 ms; T_{ZQ} = 143.8 ms; and T_{DQ} = 143.8 s across all spectra. The values of ν_1 (Hz) fitted for the spectra were: 12 (power attenuation a; 63 dB), brown line, hexagons; 14 (61 dB), yellow line, open triangles; 18 (59 dB), pink line, angled triangles; 21 (57 dB), blue line, solid diamonds; 30 (55 dB), purple line, inverted triangles; 38 (53 dB), green line, solid triangles; 48 (51 dB), red line, discs; and 60 (49 dB), black line, solid squares. The inset shows an expanded view of the fit of Eq. (13) to each data set.

3. Results

Fig. 1 shows the intensity envelopes derived from spectral deconvolution at 61.42 MHz obtained from selectively irradiating, in steps of 25 Hz over a broad range of frequencies, a sample of D_2O in gelatin (50% w/v) that had been stretched with an elongation factor of 0.7 (1.7 times the original length). The maximum suppression (minimum in the envelope of peak integrals) was exactly at the central frequency between the two components of the quadrupolar doublet. Suppression was also evident when irradiation was applied across the frequencies on either side of each of the peaks; but only when the power was very low was the suppression greater than at the central frequency. For the given extent of stretching, the difference in frequency between the two ^{2}H spectral peaks was 600 Hz; and half of this value was entered as the quadrupolar splitting, ν_Q, in Eq. (13). The inset of Fig. 1 shows an expanded view of the data (symbols) and the fits to Eq. (13) all with the same values of the relaxation times. The value of $\Delta\nu_{1/2}$ for the fitted data of the central inverted peak ranged from ~4.5 Hz at the highest RF field to ~1 Hz at the lowest.

A separate sample of gelatin (50% w/v) stretched by a factor of 0.7, and recording the spectra at 76.77 MHz, yielded a value of ν_Q = 340 Hz, and T_{ZQ}= 180 ± 9 ms, T_{DQ} = 76 ± 4 ms, T_1 = 128 ± 7 ms (<~5% coefficients of variation) and $\Delta\nu_{1/2}$ = 3.6 Hz; the predicted value was 4.8 Hz, using the theory given in Section 4 (Eq. (18)) with ν_1 = 4.8 Hz.

The fitting of Eq. (13) to data like those shown in Fig. 1 entailed an iterative approach coupled with nonlinear regression, used with only a subset of the six parameters ($\nu_1, R_1, R_2, R_3, R_{ZQ}$, and R_{DQ}) floated at any one time. The manual multi-parameter fitting was aided by six rules that were discovered empirically and are illustrated in Fig. 2, where only one of the two lateral troughs and the central dip are shown: (1) decreasing ν_1 (decreasing B_1 power) elevates the whole *z*-spectrum; (2) decreasing R_1 depresses the shoulders and depresses the level of the minimum of the central dip and the satellite troughs (in other words, equivalent to moving the central section of the spectrum down *en bloc*; (3) decreasing R_2 elevates the lateral shoulder of each trough while having an imperceptible effect on the minimum value of the central dip; (4) decreasing R_3 elevates the medial shoulder of each trough while having an imperceptible effect on the minimum value of the central dip; (5) decreasing R_{ZQ} symmetrically elevates the minimum of each satellite trough, leaving the central dip virtually unchanged; and (6) decreasing R_{DQ} depresses the minimum of the central dip, leaving the satellite troughs virtually unchanged. Note especially, the virtual independence of the shape changes in the two inverted peaks when the values of either R_{ZQ} or R_{DQ} were varied; R_{ZQ} changed the trough and not the central dip, while R_{DQ} changed the central dip and not the trough.

The values of T_1 and T_2 of HDO in the gels were known to depend on concentration and not on the extent of stretching [3]. For example, in one series of experiments T_1 for 50% and 100% gels were 99 ± 5 ms, 50 ± 3 ms and for T_2 it was 39 ± 2 ms and 15 ± 1 ms, respectively.

The data in Fig. 1 for which ν_Q was obviously very close to 300 Hz were from a sample for which the T_1 value was 100.1 ± 5.0 ms, estimated separately from an unstretched sample. By using these values, the other parameter values were adjusted iteratively and ν_1 = 38 Hz; T_2 = 40.7 ms; T_{ZQ} = 143.8 ms; and T_{DQ} = 143.8 s. Then these parameter values were held constant and other values of ν_1 were estimated by fitting to the remainder

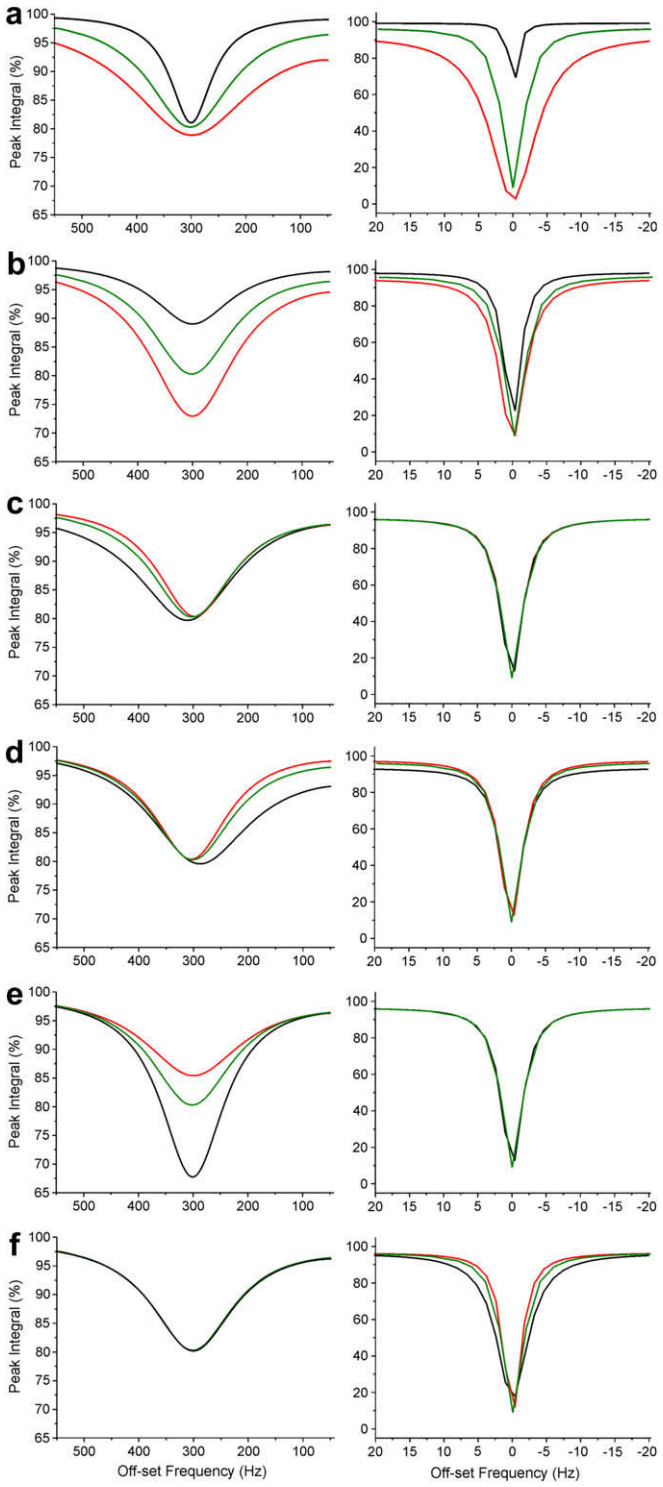

Fig. 2. The shimming-like approach to fitting Eq. (13) to a typical ^{2}H NMR saturation envelope (*z*-spectrum; % integral of control spectrum) from HDO, in stretched gelatin gel. Only the left hand trough and the central dip are shown from Fig. 1. The green line was the original fit from the green line in Fig. 1, the black line was the simulation where the respective mean parameter value was increased by 50% and the red line was when the parameter was decreased by 50%. The parameters varied for each pair of panels were: a, v_1; b, R_1; c, R_2; d, R_3; e, R_{ZQ}; f, R_{DQ}.

of the upper to lower spectra, as indicated in the caption of Fig. 1; the values of v_1 corresponded closely, in reverse order, to the actual experimental attenuation values that were applied to vary the extent of saturation of magnetization. The attenuation values were 63, 61, 59, 57, 55, 53, 51, and 49 dB; and for the latter two data sets, the frequency offsets were varied over the small range of ±50 Hz around the centre frequency.

Fig. 3 shows steady-state irradiation envelopes obtained from two gels (at 30% and 50% w/v gelatin concentrations) that were subjected to a range of extents of stretching to illustrate the effect that increasing anisotropy has on the *z*-spectra. This gave a range of values of the quadrupolar splitting from v_Q = 0–400 Hz, that varied linearly with the extent of stretching, as previously reported [3–6].

Eq. (13) was fitted to these data using a fixed value of all the relaxation parameters focussing on the data set for which v_Q = 200 Hz; the fact that T_1 must always be greater than T_2 was a constraint used in the routine analysis of the data. Then the rest of the spectra were simulated using Eq. (13) by only changing the estimate of v_Q that was obtained by nonlinear regression. An example of the fits in the central region of the envelope is shown in the inset of Fig. 3.

4. Discussion

4.1. Fitting

While it might have been expected that the values of v_1 in Fig. 1 could be calculated from a knowledge of the duration, t_p, of a $\pi/2$ pulse ($\pi/2 = \gamma\ B_1\ t_p = \omega_1\ t_p$; and the attenuation factor is equal to $10^{-a/20}$ where a is the value of the attenuation in dB) it transpired that the most successful data fitting was achieved when this value was 'floated' and the original attenuation factor only guided the choice of an initial estimate.

Fitting of Eq. (13) to the data by floating all seven parameters was unsuccessful, but using a subset of two or three parameters was possible with the nonlinear regression function (NonlinearRegress) in *Mathematica*. While it was possible to measure the various relaxation times using the pulse sequences described in Section 2.3.2, it also transpired that variations from one gel sample to another meant that the values were only suitable as initial estimates for *de novo* regression of the whole function (Eq. (13)), using the approach presented above. The fact that a single set of relaxation parameter values described closely all the spectra in Fig. 1 (apart from v_1 which was varied) was a convincing affirmation of the theory.

The value of the residual quadrupolar coupling constant, v_Q, of the HDO spectrum, varied linearly with the extent of stretching the gel, as seen in our previous studies [3–6]. The fact that estimates of relaxation parameters derived from one spectrum led to simulations that fitted very closely to the other spectra, with changes only to the value of v_Q, was again notable affirmation of the applicability of the theory to the present spin system.

Finally, it was noted that very similar spectral simulations resulted if the relaxation times were varied as a set, by keeping their relative values the same; in other words if they were all changed by the same multiplicative, scalar factor. The range of this scalar extended over many orders of magnitude (see more below). This peculiar property of Eq. (13), together with the six rules noted in Section 3, made the iterative fitting process much simpler than might have been anticipated. After a set of values had been obtained, the fitted value of T_1 was scaled to be the same as that measured experimentally in a similar sample of gelatin. Then all the other relaxation time estimates were multiplied by this same scalar factor. Specifically, for the simulations carried out for Fig. 2, the scalar multiplier was ranged from 0.25 to $>\sim 10^7$ and the curves almost completely overlay each other. This is related to the fact that saturation was almost complete (see section below Eq. (19)).

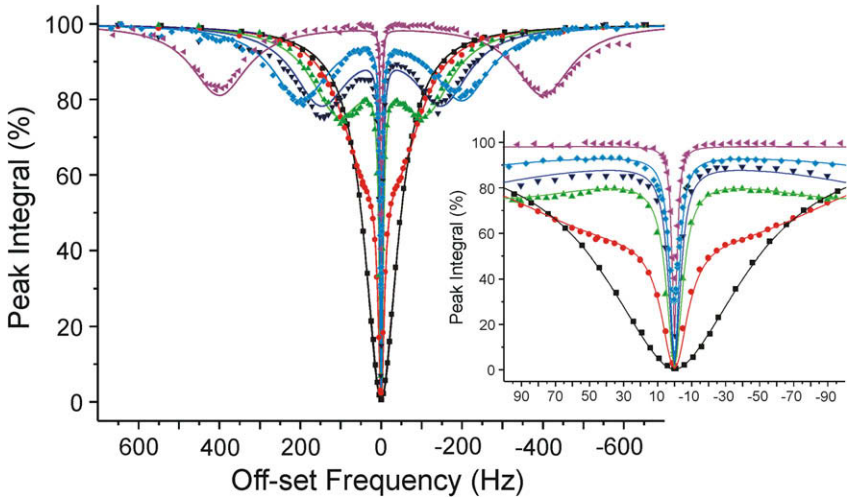

Fig. 3. ^{2}H NMR (61.422 MHz) saturation envelopes (*z*-spectrum; % integral of control spectrum) from HDO in stretched and unstretched gels made from gelatin, with various extents of stretching; the dependence of the shape of the envelope on ν_Q while keeping relaxation-rate constants and ν_1 constant, is shown. The envelopes were derived by changing the offset frequency of the applied RF irradiation on the total ^{2}H NMR signal intensity (integral) of HDO, while the corresponding starting spectra were obtained without any selective irradiation. The two samples of gelatin were prepared from 30% and 50% (w/v) bovine gelatin with 100% (w/v) pure D_2O. The six data sets (symbols) were recorded with increasing extents of stretching that led to the corresponding residual quadrupolar couplings (Hz) with fitted lines according to Eq. (13) as follows: ν_Q = 0.0 Hz, black line, solid squares; ν_Q = ~50 Hz, red line, solid discs; ν_Q = 100 Hz, green line, solid triangles; ν_Q = 140 Hz, dark blue line, inverted solid triangles; ν_Q = 200 Hz, light blue line, solid diamonds; ν_Q = 390 Hz, pink line, angled triangles. The parameter values that were applied to each data set to simulate the *z*-spectra were in all cases: T_1 = 100.1 ms; T_2 = 57.9 ms; $(1/R_3) = T_3$ = 51.7 ms; T_{ZQ} = 146.9 ms; T_{DQ} = 124.7 s, and the power of the RF field ν_1 = 38 Hz. The inset is an expansion of the central dip of the *z*-spectrum (symbols), and the simulations (solid lines) that give an indication of the overall 'goodness' of the fit for which all parameter values were the same except for ν_Q.

4.2. Tensorial relaxation rates

The idea that the transverse relaxation time of the higher rank tensors $T_{2,\pm1}$ might be different from that of $T_{1,\pm1}$ is plausible on the basis of a physical interpretation of the 'shapes' of the respective tensors (e.g., [32]). The different tensors are likely to have different interactions with their surrounding lattice, but no experimental evidence appears to exist in the literature that this is so. However, in a theoretical study by Eliav and Navon [34] it was shown that dipolar interactions of quadrupolar nuclei with spin 3/2 nuclei can lead to relaxation rates that depend on the rank of the tensor, in addition to the dependence on the coherence that results from the modulation of the quadrupolar interaction.

In the fitting of Eq. (13) to the data in Fig. 1 best fits were obtained with $T_2 = 1/R_2$ and $T_3 = 1/R_3$ having the same value (40.7 ms), whereas for Fig. 2 the best fit was obtained with two different, but similar values, 57.9 ms and 51.7 ms, respectively. In general these values are close to those directly measured experimentally (e.g., 39.2 ± 2 ms for a 50% w/v gel). This interesting aspect of the work begs further investigation.

4.3. Previous conceptualization

The direct continuous slow passage technique is the context in which the idea of double quantum transitions was first mooted [35]. The experiment can be viewed as one in which formally forbidden transitions are "over driven" by using an intense RF field [36]. More recent work using pulsed RF fields, entails the concept of multiple-quantum coherence that must be detected indirectly in a two-dimensional spectrum.

4.4. Further dissection of z-spectra

In the present one-dimensional experiments, the system was overdriven by a relatively intense selective RF field prior to recording the FID, so the experiment is analogous to the previously mentioned older continuous-wave methods [35] and more recent pulsed methods on solids [19–22]. In the latter work, it was inferred that the dependence of the intensity of the double quantum transition on RF frequency varies as a function of $1/\omega_1^4$. This can be seen from the following analysis: the dependence of the central inverted peak intensity, M_z, of the saturation envelope on the saturating RF power (that is proportional to ω_1) under the conditions where the offset frequency $\delta\omega$ and ω_1 are $<<\omega_Q$, and with the usual assumption (experimentally testable) that $\omega_1^2 T_1 T_2 >> 1$, and $\omega_1^2 T_1 T_{DQ} >> 1$ is,

$$M_z = \langle \hat{I}_z \rangle = M_{eq} \frac{1 + (2\delta\omega T_{DQ})^2}{1 + (2\delta\omega T_{DQ})^2 + \left(\frac{\omega_1}{\omega_Q}\right)^2 \omega_1^2 T_1 T_{DQ}} \tag{15}$$

where the terms in Eq. (15) are defined above. Note the dependence of the signal intensity on, amongst other parameters, the double quantum relaxation time T_{DQ}. Furthermore, the dependence on the offset is twice that obtained for a single quantum transition (Abragam [37], steady-state solution of the Bloch equations) indicating a double quantum transition.

When the saturating RF field is applied on resonance such that $\delta\omega = 0$, Eq. (15) reduces to,

$$M_z = \langle \hat{I}_z \rangle = M_{eq} \frac{1}{1 + (\frac{\omega_1}{\omega_Q})^2 \omega_1^2 T_1 T_{DQ}} \tag{16}$$

and when $\omega_1^4 T_1 T_{DQ} / \omega_Q^2 >> 1$ the equation further approximates to,

$$M_z = \langle \hat{I}_z \rangle \approx M_{eq} \frac{\omega_Q^2}{\omega_1^4 T_1 T_{DQ}} \tag{17}$$

Thus, the $1/\omega_1^4$ dependence that is indicative of double quantum (bi-photonic) transitions as suggested previously [19–22,35] is evident.

It is also informative to derive an expression for the dependence of the width-at-half-height $\Delta\nu_{1/2}$ of the up righted dip, as is often presented in *z*-spectra. This was done by solving (using the function Solve in *Mathematica*) for the value of $\delta\omega$, on equating 1 minus the right-hand sides of Eqs. (16) and (17). Thus

$$\Delta\omega_{1/2} = \left(\frac{1}{T_{DQ}}\right)\sqrt{1+\left(\frac{\omega_1}{\omega_Q}\right)^2\omega_1^2 T_1 T_{DQ}} \tag{18}$$

which, when $\omega_1^2 T_1 T_{DQ} >> 1$, further approximates to

$$\Delta\omega_{1/2} \approx \frac{\omega_1^2}{\omega_Q}\sqrt{\frac{T_1}{T_{DQ}}} \tag{19}$$

The result in Eq. (19), when combined with the values obtained for the relaxation times (see captions of Figs. 1 and 3) provides a theoretical basis to the empirically found result, reported in the beginning of the current section, that the line shape of the central dip depends on the ratio of the relaxation times and not on their absolute values. However, as noted earlier, the *z*-spectrum scale may depend on the absolute values of the relaxation times. Numerical simulations indicated that similar trends hold for the troughs under saturation conditions: $\omega_1^2 T_1 T_2 >> 1$ and $\omega_1^2 T_2 T_{ZQ} >> 1$; viz., the signal depends linearly on RF power and $1/\sqrt{T_2}$ and a linear combination of $\sqrt{T_1}$ and $\sqrt{T_{ZQ}}$. These dependencies help explain the lack of change of the line shape of the troughs as well as that of the overall line shape, as long as the ratio of the relaxation times is held constant. This result is known for spins in liquids [37].

In the situation when $\omega_Q = 0$, such as with HDO in the gel when it is not stretched, the matrix in Eq. (13) decomposes into two submatrices of first and second rank tensors; i.e., they contain no cross terms between them and are said to 'not mix'. Therefore M_z reduces to the conventional solution of the Bloch equations:

$$M_z = \langle \hat{I}_z \rangle = M_{eq}\frac{1+(\delta\omega T_2)^2}{1+(\delta\omega\ T_2)^2+\omega_1^2 T_1 T_2} \tag{20}$$

and the width-at-half-height (in Hz) of the *z*-spectrum approximates to,

$$\Delta\nu_{1/2} \approx (1/\pi)\omega_1\sqrt{\frac{T_1}{T_2}} \tag{21}$$

Hence, under most practical conditions the double quantum transitions will be a significant relaxation pathway when $0.01 < \omega_1/\omega_Q < 1$ and will cause the formation of the dip (inverted peak) in the centre of the *z*-spectrum.

These approximations proved to be useful guides to estimating the relative, or even absolute, values of the relaxation-rate constants (times) and may aid analysis of spectra obtained in other contexts.

5. Conclusions

We present an explanation for the form of the steady-state irradiation envelope (*z*-spectrum) of HDO in gelatin gel that is partially aligned by stretching. Quantification of the contributions of the various eigenstates to the final single-quantum magnetization employed measurements of the relaxation times of each of these states. Maximal suppression of the two components of the residual quadrupolar doublet by irradiation at the centre frequency between these two peaks can be attributed to saturation of the double quantum (also called bi-photonic) Boltzmann system. Applications of this phenomenon may arise in vivo with partially aligned fibrous tissues (e.g., [12,14–18]) like those in joints, tendons and the sclera of the eye. We also note that some of the water suppression that has already been reported to occur in magnetization-transfer-contrast experiments in vivo may be attributed to multiple-quantum (multi-photon) processes.

Acknowledgments

The work was funded by a Discovery Project grant from the Australian Research Council. We thank Gelita, Brisbane, QLD for the gift of gelatin. Professor Alex Bain is thanked for valuable comments and discussions.

References

[1] K.M. Ward, A.H. Aletras, R.S. Balaban, J. Magn. Reson. 143 (2000) 79–87.
[2] E. Vinogradov, S. Zhang, A. Lubag, J.A. Balschi, A.D. Sherry, R.E. Lenkinski, J. Magn. Reson. 176 (2005) 54–63.
[3] P.W. Kuchel, C. Naumann, J. Magn. Reson. 192 (2008) 48–59.
[4] P.W. Kuchel, B.E. Chapman, N. Müller, W.A. Bubb, D.J. Philp, A.M. Torres, J. Magn. Reson. 180 (2006) 256–265.
[5] C. Naumann, W.A. Bubb, B.E. Chapman, P.W. Kuchel, J. Am. Chem. Soc. 129 (2006) 5340–5341.
[6] C. Naumann, P.W. Kuchel, J. Phys. Chem. 112 (2008) 8659–8664.
[7] S. Vega, A. Pines, J. Chem. Phys. 66 (1977) 5624–5644.
[8] S. Vega, J. Chem. Phys. 68 (1978) 5518–5527.
[9] S. Vega, T.W. Shattuck, A. Pines, Phys. Rev. A 22 (1980) 638–661.
[10] G. Bodenhausen, R.L. Vold, R.R. Vold, J. Magn. Reson. 37 (1980) 93–106.
[11] G. Jacquard, S. Wimperis, G. Bodenhausen, J. Chem. Phys. 85 (1986) 6282–6293.
[12] U. Eliav, H. Shinar, G. Navon, J. Magn. Reson. 98 (1992) 223–229.
[13] I. Furo, B. Halle, Mol. Phys. 76 (1992) 1169–1197.
[14] U. Eliav, G. Navon, J. Magn. Reson. B 103 (1994) 19–29.
[15] U. Eliav, G. Navon, J. Magn. Reson. 137 (1999) 295–310.
[16] U. Eliav, G. Navon, J. Magn. Reson. 162 (2003) 166–175.
[17] U. Eliav, K. Keinan-Adamsky, G. Navon, J. Magn. Reson. 165 (2003) 276–281.
[18] U. Eliav, G. Navon, J. Magn. Reson. 190 (2008) 149–153.
[19] H. Hatanaka, T. Terao, T. Hashi, J. Phys. Soc. Jpn. 39 (1975) 835–836.
[20] H. Hatanaka, T. Hashi, J. Phys. Soc. Jpn. 39 (1975) 1139–1140.
[21] A. Pines, D.J. Ruben, S. Vega, M. Mehring, Phys. Rev. Lett. 36 (1976) 110–113.
[22] S. Vega, T.W. Shattuck, A. Pines, Phys. Rev. Lett. 37 (1976) 43–46.
[23] A. D Bain, R.M. Lynden-Bell, W.M. Litchman, E.W. Randall, J. Magn. Reson. 25 (1977) 315–326.
[24] A.D. Bain, J.S. Martin, J. Magn. Reson. 29 (1978) 125–135.
[25] C.K. Anand, A.D. Bain, Z. Nie, J. Magn. Reson. 189 (2007) 200–208.
[26] R. Ghose, Concepts Magn. Reson. 12 (2000) 152–172.
[27] N. Müller, G. Bodenhausen, R.R. Ernst, J. Magn. Reson. 75 (1987) 297–334.
[28] C.-W. Chung, S. Wimperis, Mol. Phys. 76 (1992) 47–81.
[29] P.J. Hore, J.A. Jones, S. Wimperis, NMR: The Toolkit, Oxford University Press, Oxford, 2000.
[30] R. Kemp-Harper, D.J. Philp, P.W. Kuchel, J. Chem. Phys. 115 (2001) 2908–2916.
[31] T. Eykyn, D.J. Philp, P.W. Kuchel, J. Chem. Phys. 118 (2003) 6997–7004.
[32] D.J. Philp, P.W. Kuchel, Concepts Magn. Reson. A 25 (2005) 40–52.
[33] S. Wolfram, The *Mathematica* Book, Version 6.0.2, Wolfram Media Inc., Champaign, IL.
[34] U. Eliav, G. Navon, J. Magn. Reson. A 123 (1996) 32–48.
[35] S. Yatsiv, Phys. Rev. 113 (1959) 1522–1537.
[36] R. Freeman, Concepts Magn. Reson. 10 (1998) 63–84.
[37] A. Abragam, The Principles of Nuclear Magnetism, Oxford University Press, Oxford, UK, 1978.